nature geoscience

Article

https://doi.org/10.1038/s41561-024-01466-6

Substantial contribution of slush to meltwater area across Antarctic ice shelves

Received: 3 July 2023

Accepted: 10 May 2024

Published online: 27 June 2024

Check for updates

Rebecca L. Dell [1] ✉, Ian C. Willis [1], Neil S. Arnold [1], Alison F. Banwell [1,2] & Sophie de Roda Husman [3]

Surface melting occurs across many of Antarctica's ice shelves, mainly during the austral summer. The onset, duration, area and fate of surface melting varies spatially and temporally, and the resultant surface meltwater is stored as ponded water (lakes) or as slush (saturated firn or snow), with implications for ice-shelf hydrofracture, firn air content reduction, surface energy balance and thermal evolution. This study applies a machine-learning method to the entire Landsat 8 image catalogue to derive monthly records of slush and ponded water area across 57 ice shelves between 2013 and 2021. We find that slush and ponded water occupy roughly equal areas of Antarctica's ice shelves in January, with inter-regional variations in partitioning. This suggests that studies that neglect slush may substantially underestimate the area of ice shelves covered by surface meltwater. Furthermore, we found that adjusting the surface albedo in a regional climate model to account for the lower albedo of surface meltwater resulted in 2.8 times greater snowmelt across five representative ice shelves. This extra melt is currently unaccounted for in regional climate models, which may lead to underestimates in projections of ice-sheet melting and ice-shelf stability.

Ice-shelf surface meltwater is stored predominantly as either ponded water (lakes) or slush (saturated firn or snow) (Supplementary Figs. 1 and 2). Slush can be a precursor to ponded water if meltwater fills available pore space in the firn faster than it can drain away. If slush or ponded meltwater is advected horizontally along topographic gradients, it will alter the loading on an ice shelf, which may cause it to flex[1]. In addition, surface meltwater ponding may result in hydrofracture and contribute to ice-shelf collapse, as previously observed[2] and modelled[3,4] for the Larsen B Ice Shelf. When slush or ponded water refreezes, it can form impermeable ice horizons or ice lenses, driving a reduction in the firn air content (FAC) of an ice shelf and resulting in increases in surface meltwater ponding in subsequent years[5–8].

Furthermore, ponded water and slush exert important controls on the surface energy balance of an ice shelf through the positive melt–albedo feedback[9] and through the release of latent heat during refreezing[10]. Thus, given the importance of slush and ponded water for a range of ice-shelf processes, it is imperative that recent spatiotemporal variations in their areas be investigated to inform continental-scale regional climate and ice-dynamical models that are used to project the future behaviour of ice sheets in our warming world.

Over recent years, studies have utilized optical satellite imagery to investigate trends in surface meltwater ponding on Antarctica's ice shelves. These studies have applied threshold-based techniques[11–15] or machine-learning (ML) methods[16–19] to quantify surface meltwater areas. However, no peer-reviewed study has mapped meltwater area across all Antarctic ice shelves across multiple seasons. Furthermore, all but two studies[19,20] to date have mapped only ponded water, not slush, meaning slush has been considered for only a select number of ice shelves. This is, in part, due to difficulties in mapping this surface class, which is spectrally similar to many other surface types, including ponded water, snow and blue ice[13,19]. While threshold-based methods may be applicable for slush detection across individual ice shelves

[1]Scott Polar Research Institute, Cambridge, UK. [2]Cooperative Institute for Research in Environmental Sciences, University of Colorado, Boulder, CO, USA. [3]Department of Geoscience and Remote Sensing, Delft University of Technology, Delft, the Netherlands. ✉e-mail: rld46@cam.ac.uk

and for specific melt seasons (as shown, for example, on the Nansen ice shelf in ref. 20), they are not applicable for extrapolation across all ice shelves and through multiple melt seasons due to the confusion between slush and other spectrally similar surface types[13,19].

In this Article, we use a random forest classifier[19] (Methods) to map slush and ponded water areas across 57 ice shelves during the austral summers (November–March) of 2013–2021. All ice shelves documented by ref. 21 with an area >700 km^2 were selected for this study, except Conger–Glenzer, which was disregarded as its collapse in March 2022[22,23] was seemingly unrelated to surface meltwater ponding and hydrofracture[23]. The classifier is applied to Landsat 8 Collection 1 Tier 2 scenes over the study period (regardless of cloud cover) to produce monthly surface meltwater-area products at a 30 m resolution. In addition, we produce maximum composite surface meltwater-area products for the full study period (Methods). Through the inclusion of slush, these monthly and maximum composite-area products provide a long-term record of all surface meltwater across all Antarctic ice shelves. From this dataset, spatiotemporal patterns in the onset, cessation, duration and area of surface meltwater extent (ponds and slush) between 2013 and 2021 are investigated. To examine how these patterns may be related to ice-shelf FAC, we analyse the products alongside existing modelled FAC data[24,25]. We also calculate the influence of the observed spatiotemporal patterns of pond and slush areas on the ice-shelf albedo and the resultant effects on solar radiation absorption and melt rates.

For continental- and regional-scale analysis, we investigate trends in surface meltwater extent from November to February only to remove the effect of bias where ice shelves have a lack of available imagery in March. On the continental scale, the total surface meltwater area is greatest in January of each melt season, ranging from a minimum January total area of 3.1×10^3 km^2 in 2021 to a maximum January total area of 6.0×10^3 km^2 in 2017 (Fig. 1a). For all melt seasons, total meltwater areas increase rapidly between November and January, before decreasing between January and February. When considered separately, both ponded water and slush usually reach their greatest areas in January; the exception is the 2014/2015 melt season, when ponded water area peaked in January but slush area peaked in December (Fig. 1a). Excluding this anomalous 2014/2015 melt season, the areas of slush and ponded water increase and decrease synchronously over each melt season, with the January peak in slush area always exceeding the January peak in ponded water area. This is most notable in the 2015/2016 melt season, when the slush area was almost two times greater than the ponded water area (Fig.1a). When all monthly meltwater areas (ponded water and slush) are stacked to produce a maximum composite over the full study period, the total area summed across the continent is 1.7×10^4 km^2. Of this maximum composite, 63% of the total meltwater area is classified as having been both slush and ponded water, 20% is classified as having only ever been slush, and 17% is classified as having only ever been ponded water.

The regions with the greatest maximum composite total meltwater areas are the neighbouring Dronning Maud Land and Amery Region (Fig. 2). By contrast, the Amundsen Sea and Victoria Land regions have the lowest maximum composite total meltwater areas (Fig. 2). The highest total meltwater years are identified as 2019/2020 for the Antarctic Peninsula and Wilkes Land regions on opposite sides of the continent, 2016/2017 for Dronning Maud Land and 2018/2019 for the Amery Region (Fig. 1b–i). In the Antarctic Peninsula, four of the eight melt seasons (2013/2014, 2014/2015, 2015/2016 and 2017/2018) are characterized by higher total meltwater areas in February than in January (Fig. 1b). This is also seen in Dronning Maud Land for 2016/2017 and 2020/2021, in Wilkes Land for 2015/2016 and 2016/2017 and in the Amery Region for 2017/2018 (Fig. 1d–f). In the Ross Sea region, total meltwater areas are always greatest in December[26] (Fig. 1h).

The changing proportion of slush versus ponded water within melt seasons varies from year to year and between regions. For example, in Dronning Maud Land, every melt season is characterized by a decrease in the proportion of slush between January and February, and in some cases, this decrease begins in December. This is matched by an increase in ponded water area between January and February across all melt seasons (excluding 2015/2016, 2017/2018, and 2018/2019). Across the Antarctic Peninsula, between 2013/2014 and 2016/2017, the proportion of slush decreased from December onwards, whereas the proportion of slush fell from November onwards in 2017/2018. In 2019/2020 and 2020/2021, the proportion of slush fell from November to January and then increased into February. By contrast, in 2018/2019, the proportion of slush peaked later in the melt season, in January.

The proportion of pixels only ever classified as slush within the maximum composite meltwater-area products is greatest in regions of East Antarctica, most notably Wilkes Land (43%) and Dronning Maud Land (30%) (Fig. 2). Both regions also have a low proportion of pixels that are only ever classified as ponded water, at 2% and 4%, respectively. By contrast, the proportion of pixels only ever classified as ponded water is greatest in West Antarctic regions, most notably the Filchner–Ronne (46%) and the Ross Sea (47%). These regions also have a low proportion of pixels that are only ever classified as slush, at 2% and 3%, respectively (Fig. 2). All regions have a majority of pixels that are classified as having been both slush and ponded water. Such pixels mean that (1) the surface is occupied by slush in one or more years but by ponded water in one or more other years, (2) within one or more melt seasons, slush precedes ponding or (3) within one or more melt seasons, a pond drains or partially refreezes, leaving behind slush.

On a smaller scale, we focus on the ice shelf within each region that is found to have the greatest monthly total meltwater coverage over the full study period (defined as the total meltwater divided by total ice-shelf area). These ice shelves are (1) Nivlisen (Dronning Maud Land), (2) Publications (Amery region), (3) Tracy Tremenchus (Wilkes Land), (4) Nansen (Victoria Land), and (5) George VI (Antarctic Peninsula). We exclude ice shelves in the remaining regions, where no ice shelf has a monthly total meltwater coverage > 2%, and we note that while Scar Inlet (the remnant of the Larsen B ice shelf) has a greater monthly total meltwater coverage than George VI, we focus on George VI as it has a much larger surface area.

Across Nivlisen, Publications and Tracy Tremenchus ice shelves, surface meltwater generally occurs towards the grounding lines in November of each melt season and progressively extends farther towards the ice fronts during the later months (Fig. 3a–c). Whereas on George VI, the surface meltwater is composed predominantly of ponded water, which forms both near to its grounded margins and in the central areas of the shelf[15], without previous formation of slush (Fig. 3e). For example, in January 2020, these ponds were widespread across the width (~25 km) of the northern section of this ice shelf. On Nansen, most of the surface meltwater is found over an area of blue ice (Fig. 3d).

The importance of slush

The dataset presented here provides a record of slush and ponded water area across Antarctic ice shelves for the 2013/2014 to 2020/2021 melt seasons. The mean area of slush across all ice shelves in January, which is when the continent-wide total meltwater area is greatest, accounts for 57% of the mean total January meltwater area. Therefore, previous studies that have focused solely on ponded water across Antarctica's ice shelves have underestimated the total area of surface meltwater by ignoring slush. It is crucial that future work map the extent of slush in addition to ponded water as slush plays key roles in (1) driving the reduction of an ice shelf's FAC[7], (2) facilitating the formation of ponded water[7], which can, in turn, cause the ice shelf to flex[1] and may drive hydrofracture and potential ice-shelf break-up[3,4] and (3) affecting an ice shelf's surface energy balance[9].

https://doi.org/10.1038/s41561-024-01466-6

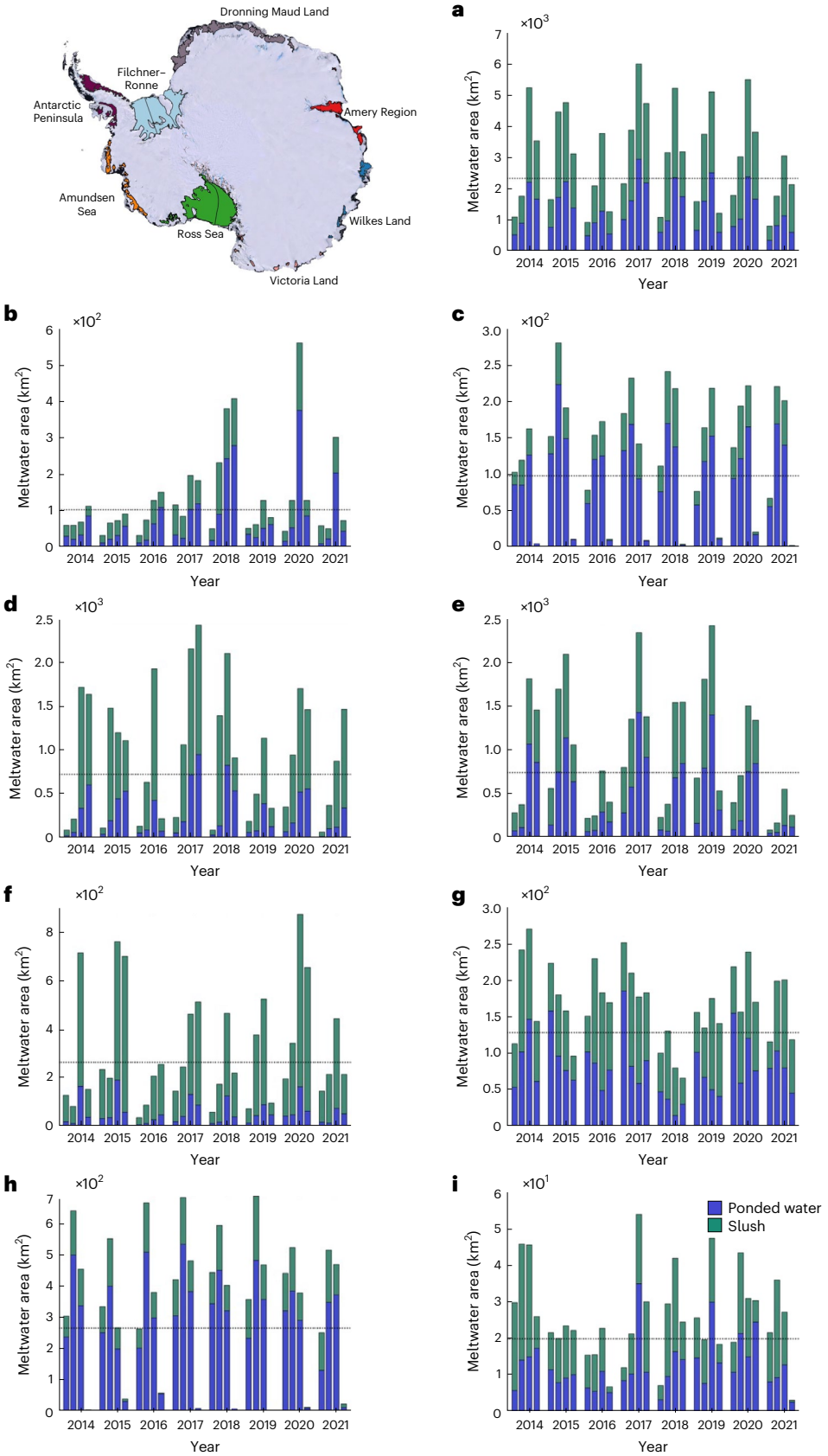

Fig. 1 | Total surface meltwater area, total ponded water area and total slush area. a–i, Summed data for all ice shelves on the continent (**a**), the Antarctic Peninsula (**b**); the Filchner–Ronne Region (**c**); Dronning Maud Land (**d**); the Amery Region (**e**); Wilkes Land (**f**); Victoria Land (**g**); the Ross Sea Region (**h**); and the Amundsen Sea Region (**i**). For each year, bars represent, from left to right, monthly data from November, December, January and February. Stacked bars are total surface meltwater area; blue is total ponded water area; green is total slush area. Dashed black lines show the respective continent or regional mean total meltwater areas. The distribution of ice shelves in each region is shown in the upper left map. Note different *y*-axis scales between plots. Tabled data provided in Supplementary Tables 1–9. Base map data from ref. 26, and ice-shelf shapefiles from a combination of refs. 41,42 (see Methods for more detail).

https://doi.org/10.1038/s41561-024-01466-6

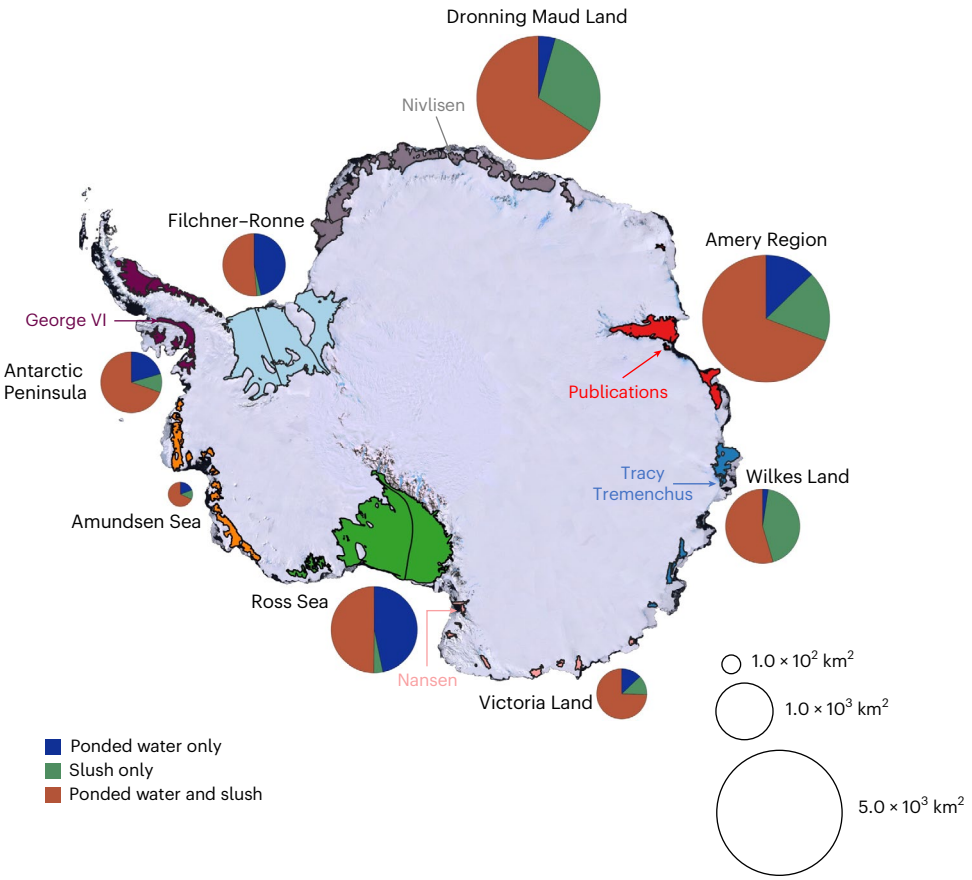

Fig. 2 | Total maximum composite surface meltwater areas for each region for 2013–2021. Total maximum composite meltwater areas are represented by proportional circles, which are colour coded to represent the proportion of surface meltwater that is only ever slush (green), only ever ponded water (blue) or both slush and ponded water (brown). Tabled data provided in Supplementary Table 10. Selected ice shelves focused on within the study are also labelled with arrows. Base map data from ref. 26 and ice-shelf shapefiles from a combination of refs. 41,42 (see Methods for more detail).

Comparison with previous studies

A study of interannual variability (2014–2020) in ponded water volume across East Antarctic ice shelves[27] finds similar patterns to those presented here, whereby 2017 is found to have the greatest volume of surface meltwater across East Antarctica, which corresponds to the continent-wide peak in slush and ponded meltwater extent across East and West Antarctica combined found here (Fig. 1).

While no continent- or region-wide studies of slush have been conducted until now, there are studies that have mapped region-wide ponded water extents, some of which we compare with our ponded water area results. Our observed total ponded water areas exceed calculations produced using thresholding methods for East Antarctica by ref. 28 and West Antarctica by ref. 29 for January 2017. When the total ponded water area from these two studies is combined, the continent-wide ponded water area in January 2017 is 1.5×10^3 km^2, while for the same period, we observe the total ponded water area across ice shelves to be approximately double this: 3.1×10^3 km^2. This variation stems from differences in the applied methodologies; in this study we utilize all imagery regardless of cloud cover, mosaicing all images within a given month, prioritizing pixels with the greatest normalized difference water index for ice ($NDWI_{ice}$) values and producing an image that shows the maximum visible monthly meltwater extent. By contrast, the threshold-based studies[28,29] utilize only images with less than 10% cloud cover (except for the Antarctic Peninsula[29], where images of up to 40% cloud cover and extending to 10 February are also included to increase image availability). These more limited image selection criteria, among other methodological differences, mean some meltwater occurrences were excluded from both previous studies.

Further, differences in ponded water extent between this and previous studies probably results from the application of an ML approach in this study compared with more conventional thresholding approaches[28,29]. Those studies acknowledge the likely exclusion of shallow ponded water from their results, owing to the difficulty in distinguishing between slush and shallow ponded water across transient boundaries[28]. By contrast, the ML approach applied in this study was designed to capture all surface meltwater, from slush to deep ponded water[19]. Shallow ponded water is therefore classified and included within the total ponded water extents calculated in our study.

Relationship with FAC

Here we compare our observed meltwater extent results against mean monthly modelled FAC (from the NASA Goddard Space Flight Center Firn Densification Model (v.2.1)[24,25]) between November and February for the years 2013–2021 (Fig. 4). We find that two FAC thresholds may be important in explaining total meltwater area (Fig.4). First, for the nine ice shelves with FAC > 21 m, total meltwater coverage (melt given as a percentage of the ice-shelf area) is consistently <1%. Second, for the 21 ice shelves where FAC < 14 m, total meltwater coverage exceeds 5% for six ice shelves: two in Wilkes Land (Tracy Tremenchus and Vincennes), two in Dronning Maud Land (Nivlisen and Roi Baudouin), one in the Amery region (Publications) and one in Victoria Land (Nansen) (Fig. 4). With FACs between 14 m and 21 m, total meltwater coverages are much lower than 5% with one exception; Wilma Robert Downer ice shelf has a maximum monthly total meltwater coverage of 4%, at a relatively high FAC of 18 m. These 14 m and 21 m thresholds reflect the availability of firn pore space, into which surface meltwater can infiltrate and flow

https://doi.org/10.1038/s41561-024-01466-6

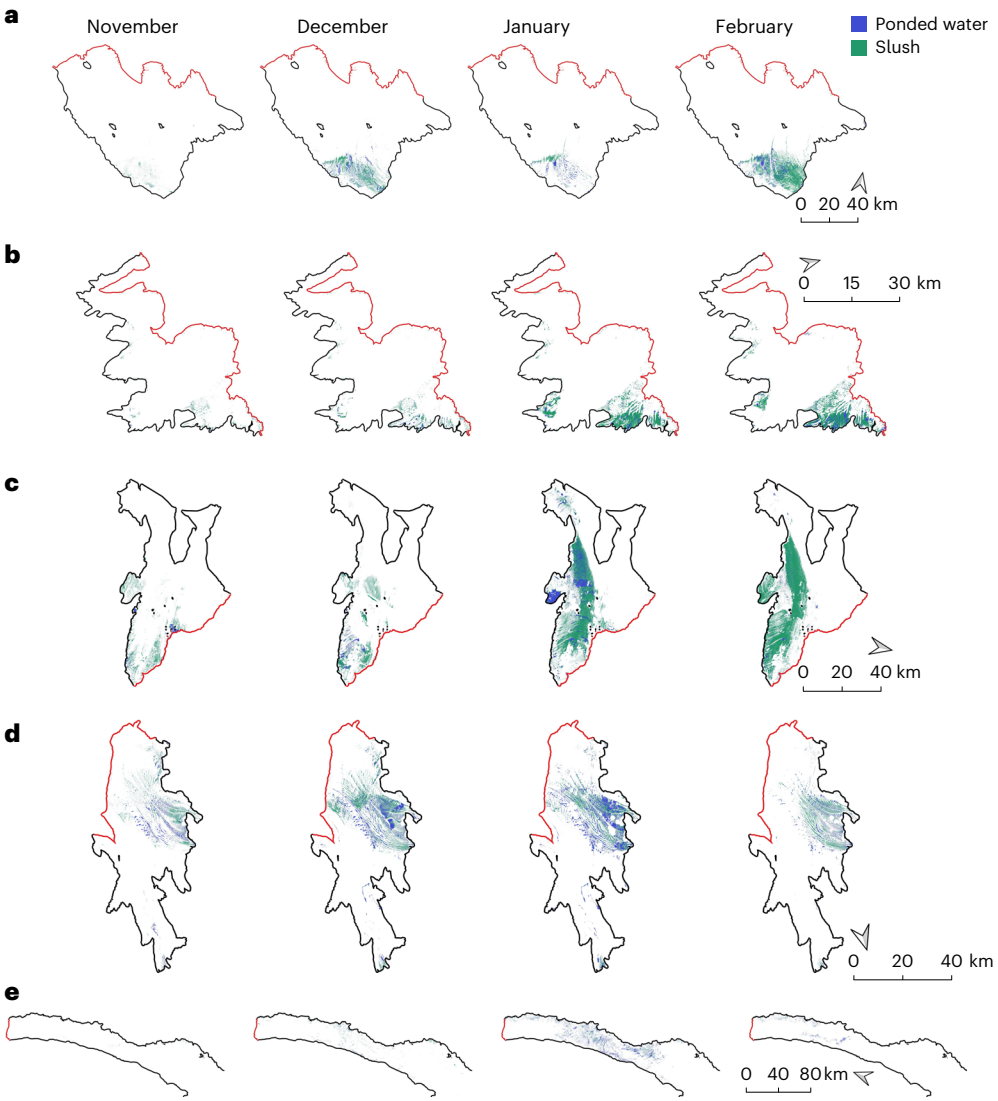

Fig. 3 | Monthly (November–February) meltwater products for selected ice shelves. For each ice shelf, the melt season with the greatest observed total monthly meltwater area is shown. **a**, Nivlisen in 2020/2021. **b**, Publications in 2014/2015. **c**, Tracy Tremenchus in 2014/2015. **d**, Nansen in 2013/2014. **e**, North George VI in 2019/2020. Note we show only north George VI here as this is where the majority of meltwater is observed. For each month, the area of slush (green) and ponded water (blue) is shown. Red boundary lines mark the ice-shelf fronts, and black boundary lines mark the ice-shelf grounding lines, following the ice-shelf outlines used for this study (see Methods for more detail). Supplementary Figs. 3–7 show zoomed-in subsets of each ice shelf for greater detail.

both laterally and vertically through the ice-shelf subsurface[30]. Where the mean FAC of an ice shelf is low (<14 m), the available pore space is limited, and slush and ponded water can form on the ice surface. However, where an ice shelf's mean FAC is high (>21 m), the majority of meltwater can be stored within its subsurface, resulting in minimal slush and ponded water formation. The FAC, and therefore meltwater storage capacity, of these ice shelves depends on the balance of accumulation versus refreezing of meltwater, refreezing of rain and firn densification processes, all of which will change in a warming climate[7,22,31].

However, regions with similar mean ice-shelf FACs (Fig. 4) show marked differences in total maximum composite meltwater areas (Fig. 2). This is most notable when comparing total maximum composite meltwater areas across the Antarctic Peninsula (mean FAC = 13.4 m, total maximum composite melt area = 1.2×10^3 km^2), Dronning Maud Land (mean FAC = 14.2 m, total maximum composite melt area = 4.8×10^3 km^2), Wilkes Land (mean FAC = 14.9 m, total maximum composite melt area = 1.7×10^3 km^2) and Amery Region (mean FAC = 13.2 m, total maximum composite melt area = 5.1×10^3 km^2). While the FACs in these regions have a relatively low spread of 1.7 m, the total maximum composite meltwater areas have a large spread of 3.9×10^3 km^2, with meltwater areas in Dronning Maud Land and Amery Region exceeding those in the Antarctic Peninsula and Wilkes Land (Fig. 2). These findings suggest that while FAC values exert a first-order control on the presence of surface meltwater ponding across Antarctica, ponding is also controlled by local factors probably not resolved by the 12.5 km × 12.5 km gridded FAC data[24,25], such as ice-lens presence[32], local topography, blue-ice exposure, proximity to nunataks and local and regional climate[28,33,34].

Impact on albedo and surface energy absorption

The presence of both slush and ponded water on an ice shelf alters the ice-shelf albedo, affecting the ice-shelf energy balance[9]. Here we adjust RACMO2.3p2[35] (RACMO) snowmelt values by the ratio of RACMO albedo to Landsat 8 albedo in areas of slush and ponded water, following ref. 33. We make these estimates for January of the year with the maximum monthly total meltwater area for our five case-study ice shelves (Publications, Tracy Tremenchus, George VI, Nivlisen and Nansen) (Table 1). We note that for each ice shelf, and for both surface meltwater categories, RACMO overestimates surface albedo, and

Table 1 | Albedo values and adjusted modelled melt for the five case-study ice shelves in January of their maximum melt years

	L8 C2 SR albedo values		RACMO albedo values (SWSU/SWSD)		RACMO snowmelt (mm w.e.)	Adjusted RACMO snowmelt (mm w.e.)
	Ponded water	Slush	Ponded water	Slush		
George VI	0.45	0.69	0.83	0.83	163.37	496.61
Nivlisen	0.48	0.65	0.83	0.83	11.05	32.96
Publications	0.52	0.73	0.82	0.78	32.19	85.23
Tracy Tremenchus	0.56	0.62	0.85	0.85	72.22	207.22
Nansen	0.52	0.69	0.79	0.79	21.71	58.20

For each ice shelf (column 1), mean Landsat 8 ponded water and slush albedo values (extracted from Landsat 8 surface reflectance (L8 C2 SR) products) are given (column 2), as are mean RACMO[35] albedo values for the corresponding pixels (column 3). Column 4 shows the mean RACMO snowmelt for all pixels that overlap with surface meltwater (identified using the classified Landsat 8 products), and column 5 shows the RACMO snowmelt adjusted for the ratio of RACMO albedo to Landsat 8 albedo for both slush and ponded water (Methods). SWSU, upwelling short-wave radiation at the surface; SWSD, downwelling short-wave radiation at the surface; w.e., water equivalent.

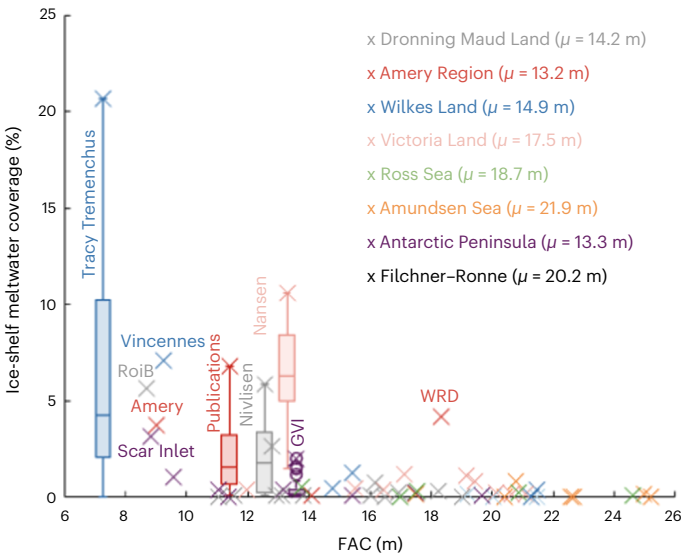

Fig. 4 | Mean ice-shelf FAC versus maximum monthly ice-shelf total meltwater coverage. Box plots (centred on the mean FAC[24,25] and showing the median ice-shelf meltwater coverage (centre line), with whiskers representing the lower and upper quartiles) for the five 'wettest' ice shelves within their regions and scatter points (mean FAC versus maximum monthly ice-shelf total meltwater coverage) for all remaining ice shelves. The five wettest ice shelves within their respective regions are labelled with vertical text, and other ice shelves with high ice-shelf total meltwater coverage are labelled with horizontal text. Mean regional modelled FACs over the full study period (μ) are given in the legend. GVI, George VI; RoiB, Roi Baudouin; WRD, Wilma Robert Downer.

therefore underestimates snowmelt (Table 1). Furthermore, we note that the resolution of RACMO does not facilitate fine-scale albedo differences between slush and ponded water, and the two surface types are therefore incorrectly prescribed near-identical albedo values. On average, by scaling original snowmelt values by the ratio of RACMO albedo values to Landsat 8 albedo values, RACMO snowmelt increases by 2.8 times its original value. This is most marked on George VI ice shelf, where adjusted snowmelt values are triple the original RACMO snowmelt values. Given that RACMO does not account for the impact of slush or ponded water on the surface albedo, our findings provide a strong motive for including this melt–albedo feedback process, for both slush and ponded water, in surface energy-balance models.

Outlook

We have presented a record of slush and ponded water across all of Antarctica's large ice shelves from 2013 to 2021 and have shown that ice-shelf FAC provides a first-order control on total meltwater area. When meltwater area is at its peak (in January of each melt season), slush accounts for, on average, 57% of the total surface meltwater area, although it exhibits marked spatial and temporal variability. As both slush and ponded water lower the albedo of the ice-shelf surface compared with surrounding bare ice and snow, solar absorption will increase, thereby generating additional melt through the melt–albedo feedback mechanism[9,36]. For our five specific ice shelves, we find that this additional melt is at least 2.8 times the modelled snowmelt in RACMO2.3p2[35], which does not currently account for the impact of slush and ponded water on the surface albedo. On this basis, previous model estimates of FAC may be overestimated as a result of underestimating melt. This would particularly be the case if the extra melt formed extensive ice layers in the firn layers[37].

Although changes in meltwater volumes on Antarctic ice shelves have been relatively small over the past four decades (1980–2021), projected atmospheric warming means that future surface meltwater production on ice shelves is expected to increase nonlinearly, and hence ice shelves are predicted to become more vulnerable to future surface meltwater-induced instability[9,38–40]. Therefore, on the basis of this current study, our recommendations for future work are twofold: (1) observational studies of surface meltwater should not ignore slush, but should map it using suitable ML methodologies[19] to fully capture ice shelves' surface meltwater areas, and (2) ice-shelf surface energy-balance models used within regional climate models should better account for the melt–albedo feedback driven by both slush and ponded water to better estimate the extra melt these surface facies generate.

Online content

Any methods, additional references, Nature Portfolio reporting summaries, source data, extended data, supplementary information, acknowledgements, peer review information; details of author contributions and competing interests; and statements of data and code availability are available at https://doi.org/10.1038/s41561-024-01466-6.

References

1. Banwell, A. F., Willis, I. C., Macdonald, G. J., Goodsell, B. & MacAyeal, D. R. Direct measurements of ice-shelf flexure caused by surface meltwater ponding and drainage. *Nat. Commun.* **10**, 730 (2019).
2. Scambos, T., Hulbe, C. & Fahnestock, M. in *Antarctica Peninsula Climate Variability: A Historical and Paleo-Environmental Perspective* (eds Domack, E. e al.) 79–92 (American Geophysical Union, 2003).
3. Banwell, A. F., MacAyeal, D. R. & Sergienko, O. V. Breakup of the Larsen B ice shelf triggered by chain reaction drainage of supraglacial lakes. *Geophys. Res. Lett.* **40**, 5872–5876 (2013).
4. Robel, A. A. & Banwell, A. F. A speed limit on ice shelf collapse through hydrofracture. *Geophys. Res. Lett.* **46**, 12092–12100 (2019).
5. Forster, R. R. et al. Extensive liquid meltwater storage in firn within the Greenland ice sheet. *Nat. Geosci.* **7**, 95–98 (2013).

6. Machguth, H. et al. Greenland meltwater storage in firn limited by near-surface ice formation. *Nat. Clim. Change* **6**, 390–393 (2016).
7. Kuipers Munneke, P., Ligtenberg, S. R. M., Van Den Broeke, M. R. & Vaughan, D. G. Firn air depletion as a precursor of Antarctic ice-shelf collapse. *J. Glaciol.* **60**, 205–214 (2014).
8. Alley, K. E., Scambos, T. A., Miller, J. Z., Long, D. G. & MacFerrin, M. Quantifying vulnerability of Antarctic ice shelves to hydrofracture using microwave scattering properties. *Remote Sens. Environ.* **210**, 297–306 (2018).
9. Trusel, L. D. et al. Divergent trajectories of Antarctic surface melt under two twenty-first-century climate scenarios. *Nat. Geosci.* **8**, 927–932 (2015).
10. Tseng, P. -H., Illangasekare, T. H. & Meier, M. F. Modeling of snow melting and uniform wetting front migration in a layered subfreezing snowpack. *Water Resour. Res.* **30**, 2363–2376 (1994).
11. Banwell, A. F. et al. Supraglacial lakes on the Larsen B ice shelf, Antarctica, and at Paakitsoq, West Greenland: a comparative study. *Ann. Glaciol.* https://doi.org/10.3189/2014AoG66A049 (2014).
12. Dell, R. et al. Lateral meltwater transfer across an Antarctic ice shelf. *Cryosphere* **14**, 2313–2330 (2020).
13. Moussavi, M. et al. Antarctic supraglacial lake detection using Landsat 8 and Sentinel-2 imagery: towards continental generation of lake volumes. *Remote Sens.* **12**, 134 (2020).
14. Arthur, J. F. et al. The triggers of the disaggregation of Voyeykov ice shelf (2007), Wilkes Land, East Antarctica, and its subsequent evolution. *J. Glaciol.* **67**, 933–951 (2021).
15. Banwell, A. F. et al. The 32-year record-high surface melt in 2019/2020 on the northern George VI ice shelf, Antarctic Peninsula. *Cryosphere* **15**, 909–925 (2021).
16. Dirscherl, M., Dietz, A. J., Kneisel, C. & Kuenzer, C. Automated mapping of Antarctic supraglacial lakes using a machine learning approach. *Remote Sens.* **12**, 1203 (2020).
17. Dirscherl, M., Dietz, A. J., Kneisel, C. & Kuenzer, C. A novel method for automated supraglacial lake mapping in Antarctica using Sentinel-1 SAR imagery and deep learning. *Remote Sens.* **13**, 197 (2021).
18. Halberstadt, A. R. W. et al. Antarctic supraglacial lake identification using Landsat-8 image classification. *Remote Sens.* **12**, 1327 (2020).
19. Dell, R. L. et al. Supervised classification of slush and ponded water on Antarctic ice shelves using Landsat 8 imagery. *J. Glaciol.* **68**, 401–414 (2021).
20. Bell, R. E. et al. Antarctic ice shelf potentially stabilized by export of meltwater in surface river. *Nature* **544**, 344–348 (2017).
21. Rignot, E., Jacobs, S., Mouginot, J. & Scheuchl, B. Ice-shelf melting around Antarctica. *Science* **341**, 266–270 (2013).
22. van Wessem, J. M., van den Broeke, M. R., Wouters, B. & Lhermitte, S. Variable temperature thresholds of melt pond formation on Antarctic ice shelves. *Nat. Clim. Change* **13**, 161–166 (2023).
23. Wille, J. D. et al. The extraordinary March 2022 East Antarctica 'heat' wave. Part II: impacts on the Antarctic ice sheet. *J. Clim.* **37**, 779–799 (2023).
24. Medley, B., Neumann, T. A., Zwally, H. J., Smith, B. E. & Stevens, C. M. Simulations of firn processes over the Greenland and Antarctic ice sheets: 1980–2021. *Cryosphere* **16**, 3971–4011 (2022).
25. Medley, B., Neumann, T., Zwally, H. J., Smith, B. E. & Stevens, C. M. NASA GSFC Firn Densification Model version 1.2.1 (GSFC-FDMv1.2.1) for the Greenland and Antarctic Ice Sheets: 1980-2021. *Zenodo* https://doi.org/10.5281/ZENODO.7054574 (2022).
26. Bindschadler, R. et al. The Landsat Image Mosaic of Antarctica. *Remote Sens. Environ.* **112**, 4214–4226 (2008).
27. Arthur, J. F. et al. Large interannual variability in supraglacial lakes around East Antarctica. *Nat. Commun.* **13**, 1711 (2022).
28. Stokes, C. R., Sanderson, J. E., Miles, B. W. J., Jamieson, S. S. R. & Leeson, A. A. Widespread distribution of supraglacial lakes around the margin of the East Antarctic Ice Sheet. *Sci. Rep.* **9**, 13823 (2019).
29. Corr, D., Leeson, A., McMillan, M., Zhang, C. & Barnes, T. An inventory of supraglacial lakes and channels across the West Antarctic Ice Sheet. *Earth Syst. Sci. Data* **14**, 209–228 (2022).
30. Montgomery, L. et al. Hydrologic properties of a highly permeable firn aquifer in the Wilkins ice shelf, Antarctica. *Geophys. Res. Lett.* **47**, e2020GL089552 (2020).
31. Donat-Magnin, M. et al. Future surface mass balance and surface melt in the Amundsen sector of the West Antarctic Ice Sheet. *Cryosphere* **15**, 571–593 (2021).
32. Hubbard, B. et al. Massive subsurface ice formed by refreezing of ice-shelf melt ponds. *Nat. Commun.* **7**, 11897 (2016).
33. Lenaerts, J. T. M. et al. Meltwater produced by wind-albedo interaction stored in an East Antarctic ice shelf. *Nat. Clim. Change* **7**, 58–62 (2017).
34. Kingslake, J., Ely, J. C., Das, I. & Bell, R. E. Widespread movement of meltwater onto and across Antarctic ice shelves. *Nature* **544**, 349–352 (2017).
35. van Wessem, J. M., van de Berg, W. J. & van den Broeke, M. R. Data set: Monthly averaged RACMO2. 3p2 variables (1979–2022); Antarctica. *Zenodo* https://doi.org/10.5281/zenodo.7760490 (2023).
36. Banwell, A. F., Wever, N., Dunmire, D. & Picard, G. Quantifying Antarctic-wide ice-shelf surface melt volume using microwave and firn model data: 1980 to 2021. *Geophys. Res. Lett.* **50**, e2023GL102744 (2023).
37. Veldhuijsen, S. B. M., van de Berg, W. J., Kuipers Munneke, P. & van den Broeke, M. R. Firn air content changes on Antarctic ice shelves under three future warming scenarios. *Cryosphere* **18**, 1983–1999 (2023).
38. Gilbert, E. & Kittel, C. Surface melt and runoff on Antarctic ice shelves at 1.5 °C, 2 °C and 4 °C of future warming. *Geophys. Res. Lett.* **48**, e2020GL091733 (2021).
39. Kittel, C. et al. Diverging future surface mass balance between the Antarctic ice shelves and grounded ice sheet. *Cryosphere* **15**, 1215–1236 (2021).
40. Lai, C. Y. et al. Vulnerability of Antarctica's ice shelves to meltwater-driven fracture. *Nature* **584**, 574–578 (2020).
41. Gerrish, L., Fretwell, P. & Cooper, P. *High Resolution Vector Polygons of the Antarctic Coastline* (7.3) [Data set] (UK Polar Data Centre, NERC, UKRI, 2020); https://doi.org/10.5285/ad7d345a-0650-4f44-b7eb-c48e1999086b
42. Mouginot, J., Scheuchl, B. & Rignot, E. *MEaSUREs Antarctic Boundaries for IPY 2007-2009 from Satellite Radar, Version 2* [Data Set]. Boulder, Colorado USA. NASA National Snow and Ice Data Center Distributed Active Archive Center. https://doi.org/10.5067/AXE4121732AD (2017).

Methods

Ice-shelf shapefiles

Antarctic ice shelves with an area >700 km^2 were used in this study[21]. The only ice shelf with an area >700 km^2 that was disregarded was Conger–Glenzer ice shelf, which collapsed in March 2022[22]. Shapefiles for each ice shelf were obtained from the SCAR Antarctic Digital Database as high-resolution vector polygons[41]. In some cases, further boundary modifications were required to separate neighbouring ice shelves, and the Making Earth System Data Records for Use in Research Environments (MEaSUREs) v.2 database was used for this purpose[42]. In other cases, multiple polygons that form part of a single ice shelf were grouped into the same shapefile where necessary (for example, for Larsen E ice shelf). Ice shelves were grouped into regions following ref. 8. Owing to computational load, both Ross and Ronne Ice Shelves were split into Ross E and Ross W, and Ronne pt.1 and Ronne Pt.2.

Scene selection and pre-processing

Within Google Earth Engine[43] (GEE), an existing method[19] was used to obtain, pre-process and mosaic Landsat 8 (Collection 1, Tier 2) scenes for the austral summers of 2013/2014 to 2020/2021, prioritizing pixels with the greatest $NDWI_{ice}$ values. Briefly summarized, these steps are as follows: (1) find all Landsat 8 Collection 1 Tier 2 images with a solar elevation >20° (regardless of cloud cover); (2) adjust pixel values that were converted to top-of-atmosphere values using the scene centre solar angle to values that better approximate per-pixel top-of-atmosphere values; (3) clip each scene to the ice-shelf boundaries; (4) apply a threshold-based rock mask, including a 1 km buffer[13]; (5) mask clouds and cloud shadows using the Landsat Band Quality Assessment bands, including a 4 km buffer[19]; (6) use the quality mosaic function within GEE to produce monthly mosaics from all available imagery, prioritizing pixels with the greatest $NDWI_{ice}$ values (note this differs from ref. 19, where 15 day mosaics were produced); and (7) apply an $NDWI_{ice}$ filter of >0.1 to extract all pixels that are probably wet. The final outputs from the preceding steps are monthly images composed of pixels with $NDWI_{ice}$ values > 0.1 only. These images are then passed to the trained random forest classifier[19].

Random forest classification

Pre-processed monthly mosaics were classified in GEE using the random forest classifier developed by ref. 19, and the classified outputs and corresponding RGB (red, green and blue) images were subsequently exported for further analysis. Pixels were classified as ponded water, slush or a variety of extraneous classes that were disregarded for the purposes of this study.

Data post-processing

Each classified monthly product was post-processed in MATLAB to remove false positive classifications caused by cloud, cloud shadows and structural damage. To remove misclassifications caused by the presence of cloud and cloud shadows, we exploit their more transient nature relative to surface meltwater, which often reforms in the same locations each melt season[19]. We adapted the method used by ref. 19, which masked out pixels classified as surface meltwater for just one time step (note time steps in ref. 19 were bi-monthly) during the full study period as it is likely that pixels with such a low meltwater persistence are false positive classifications caused by the presence of cloud/cloud shadow. For our current study, we apply a more stringent approach to mask out clouds and cloud shadows by removing pixels classified as surface meltwater for ≤2 time steps (any two months) throughout the full study period (2013–2021).

To remove misclassifications due to structural damage, pixels were masked according to surface velocities[44–47] and slope[48]. Most ice shelves were masked for surface velocities > 200 m yr^{-1}, according to the MEaSUREs velocity data, and for surface slope angles > 5%, using the Reference Elevation Model of Antarctica (REMA) Digital Elevation Model (DEM). A one-pixel buffer was added to this latter mask, which is a similar approach to the one adopted by refs. 16 and 17. A few ice shelves were masked with variations on this procedure as documented in Supplementary Table 11.

Where image availability allows, the final output is monthly (November–March inclusive) slush, ponded water and total water areas for all 57 ice shelves for each year (2013–2021); 2,003 products in total (Fig. 1). We utilized ChatGPT to assist in writing a script to check for extra file dates within our folder structure that were not required for this study.

Maximum composite meltwater-area products

Maximum composite total water areas for each ice shelf were made by stacking all available monthly products over the full study period (November 2013–March 2021). Within each maximum composite meltwater-area product, pixels were tagged as (1) only ever ponded water, (2) only ever slush, or (3) both slush and ponded water at least once during the study period. This final category identifies meltwater pixels that changed category through time.

Regional and continent-wide calculations

To identify regional trends in ice-shelf surface meltwater ponding and slush across Antarctica, the 57 ice shelves were grouped into eight regions[8]. Monthly meltwater products and maximum composite meltwater products for all ice shelves in each region were summed to produce regional monthly and maximum composite meltwater areas (Fig. 2). These regional monthly and maximum composite meltwater areas were summed to calculate Antarctic-wide meltwater areas. For these regional and continent-wide data calculations only, data from March were excluded as a lack of data from this month for some ice shelves in some years would have biased the results.

FAC data

To examine possible ice-shelf surface controls on patterns of surface meltwater, Antarctic-wide FAC data[24,25] between November 2013 and February 2021 were used. The data, from the NASA Goddard Space Flight Center Firn Densification Model (v.2.1), offer 5 day products for FAC. For atmospheric forcing, the model uses global atmospheric reanalysis, specifically MERRA-2 (Modern-Era Retrospective Analysis for Research and Applications, version 2), which is complemented by offline replay MERRA-2 runs (12.5 km horizontal resolution) over the Antarctic Ice Sheet. Melt is forced using a calibrated degree-day model[24,25,49].

For this study, we clipped the data to the area of each ice shelf, and for each ice shelf, mean FAC values were calculated for November to February. The mean FAC data were compared with the monthly total meltwater-area products for each ice shelf (Fig. 4). Note that both Ross and Ronne Ice Shelves were analysed in two halves, as per their ice-shelf shapefiles.

Extra solar radiation and melt calculations

To examine the surface meltwater–albedo feedback mechanism, we used RACMO2.3p2 data[35] to estimate the extra solar radiation absorbed by both slush and ponded water for five ice shelves during January of the year with the maximum monthly total meltwater area. The method used here is similar to that of ref. 33.

First, for each ice shelf, and separately for slush and ponded water, the mean Landsat 8 albedo values and the mean RACMO albedo values were calculated. Landsat 8 albedo values for each ice shelf were calculated by selecting the least cloudy Landsat 8 Collection 2 surface reflectance image from the relevant January, clipping it to the relevant ice-shelf extent and calculating the broadband albedo values for each pixel[50]. The corresponding Landsat 8 Collection 1 top-of-atmosphere image was also classified within GEE (as in the preceding, excluding the creation of a monthly mosaic). From here, the mean slush and

ponded water surface albedo values were extracted from the surface reflectance image (using the classified outputs from the corresponding top-of-atmosphere image). RACMO albedo values were calculated by dividing upwelling short-wave radiation at the surface by downwelling short-wave radiation at the surface. Mean RACMO albedo values for slush and ponded water were then extracted, again using the classified outputs from the Landsat 8 top-of-atmosphere image.

For each ice shelf, the extra melt generated by albedo differences from observed areas of slush and ponded water were then estimated by calculating the ratio of RACMO albedo values to Landsat 8 albedo values. This ratio was then multiplied by the snowmelt product from RACMO (calculated as the mean snowmelt of any RACMO cells that overlap pixels classified as slush and ponded water in the Landsat 8 products), under the assumption that all additional energy would lead to surface melting[33]. The final adjusted snowmelt values (in mm w.e.) were then compared with RACMO's original snowmelt values.

Data availability

Satellite data used in this study are freely available and can be obtained from https://earthengine.google.com/ (Landsat Imagery), https://nsidc.org/data/nsidc-0484/versions/2 (MEaSUREs Velocity Data) and https://data.pgc.umn.edu/elev/dem/setsm/REMA/ (REMA DEM). RACMO2.3p2 data can be downloaded from https://zenodo.org/record/7845736#.ZFzn_%20-zMLPZ%20and%20reprojected%20to%20EPSG%20303 and FAC data from https://zenodo.org/record/7054574#.Y0_yqOzMLPY. The final ice-shelf shapefiles are available via the Cambridge Apollo Repository at https://doi.org/10.17863/CAM.108421; these shapefiles were made using a combination of shapefiles from the SCAR Antarctic Digital Database (https://doi.org/10.5285/0a6d85d7-fc9c-4d68-a58d-e792f68ae9f4) and the MEaSUREs v.2 database (https://nsidc.org/data/nsidc-0709/versions/2) (Methods). The final, post-processed surface meltwater products produced for this study are also available via the Cambridge Apollo Repository (https://doi.org/10.17863/CAM.108421). The script used to better approximate per-pixel top-of-atmosphere values is available at https://groups.google.com/g/google-earth-engine-developers/c/Yv45HWL14d4/m/ce583P2SBgAJ.

Code availability

The Google Earth Engine and MATLAB code used to generate and post-process the observed surface meltwater dataset in this study is available at https://doi.org/10.17863/CAM.108421.

References

43. Gorelick, N. et al. Google Earth Engine: planetary-scale geospatial analysis for everyone. *Remote Sens. Environ.* **202**, 18–27 (2017).
44. Rignot, E., Mouginot, J. & Scheuchl, B. *MEaSUREs InSAR-Based Antarctica Ice Velocity Map, Version 2* [Data Set]. Boulder, Colorado USA. NASA National Snow and Ice Data Center Distributed Active Archive Center. https://doi.org/10.5067/D7GK8F5J8M8R (2017).
45. Rignot, E., Mouginot, J. & Scheuchl, B. Ice Flow of the Antarctic Ice Sheet. *Science* **333**. https://doi.org/10.1126/science.1208336 (2011).
46. Mouginot, J., Scheuchl, B. & Rignot, E. Mapping of Ice Motion in Antarctica Using Synthetic-Aperture Radar Data. *Remote Sens.* **4**. https://doi.org/10.3390/rs4092753 (2012).
47. Mouginot, J., Rignot, E., Scheuchl, B. & Millan, R. Comprehensive annual ice sheet velocity mapping using Landsat-8, Sentinel-1, and RADARSAT-2 data. *Remot Sens.* **9**, 364 (2017).
48. Howat, I. M., Porter, C., Smith, B. E., Noh, M.-J. & Morin, P. The Reference Elevation Model of Antarctica. *The Cryosphere* **13**, 665–674 (2019).
49. van den Broeke, M., Bus, C., Ettema, J. & Smeets, P. Temperature thresholds for degree-day modelling of Greenland ice sheet melt rates. *Geophys. Res. Lett.* **37,** L18501 (2010).
50. Liang, S. Narrowband to broadband conversions of land surface albedo I. *Remote Sens. Environ.* **76**, 213–238 (2001).

Acknowledgements

R.L.D. was supported by the European Space Agency, who funded her work through the Climate Change Initiative fellowship (ESA ESRIN/ contract no. 4000134462/21/I-NB). I.C.W. received financial assistance from the United Kingdom Natural Environment Research Council awarded to the University of Cambridge (grant number NE/T006234/1). A.F.B. received support from the US National Science Foundation (NSF) under awards no. 1841607 and no. 2213702 to the University of Colorado Boulder. S.d.R.H. was supported by Nederlandse Organisatie voor Wetenschappelijk Onderzoek (NWO) under grant OCENW.GROOT.2019.091. The authors thank T. Chudley for his python support when processing the FAC data, and M. van den Broeke for his advise on RACMO data. We also acknowledge the use of ChatGPT within this study, specifically in writing a script capable of checking for files within a folder collection. DEMs provided by the Byrd Polar and Climate Research Center and the Polar Geospatial Center under NSF-OPP awards 1043681, 1542736, 1543501, 1559691, 1810976, and 2129685.

Author contributions

R.L.D., I.C.W., N.S.A. and A.F.B. designed the study and interpreted the data. R.L.D. carried out all data processing for the optical surface meltwater products. S.d.R.H. downloaded and reprojected the RACMO2.3p2 data. R.L.D. wrote the manuscript and created all of the figures, with edits and assistance from all other contributing authors.

Competing interests

The authors declare no competing interests.

Additional information

Supplementary information The online version contains supplementary material available at https://doi.org/10.1038/s41561-024-01466-6.

Correspondence and requests for materials should be addressed to Rebecca L. Dell.

Peer review information *Nature Geoscience* thanks Luke Trusel, Amber Leeson and Jeremy Ely for their contribution to the peer review of this work. Primary Handling Editor: Tom Richardson, in collaboration with the *Nature Geoscience* team.